Author(s): Yuan, Xiting; Ye, Zichen; Malola, Sami; Shekhah, Osama; Jiang, Hao; Hu, Xinyan; Wang, Jian-Xin; Wang, Hong; Shkurenko, Aleksander; Jia, Jiangtao; Guillerm, Vincent; Mohammed, Omar F.; Chen, Xiaolan; Zheng, Nanfeng; Häkkinen, Hannu; Eddaoudi, Mohamed

Title: Synthesis and crystallization of a carboxylate functionalized N-heterocyclic carbene-based Au13 cluster with strong photo-luminescence

Year: 2024

Version: Published version

Chemical Science

ROYAL SOCIETY OF CHEMISTRY

EDGE ARTICLE

View Article Online
View Journal

Cite this: DOI: 10.1039/d4sc04594g

All publication charges for this article have been paid for by the Royal Society of Chemistry

Synthesis and crystallization of a carboxylate functionalized *N*-heterocyclic carbene-based Au_{13} cluster with strong photo-luminescence†

Xiting Yuan,[a] Zichen Ye,[b] Sami Malola,[c] Osama Shekhah,[a] Hao Jiang,[b] Xinyan Hu,[b] Jian-Xin Wang,[ad] Hong Wang,[d] Aleksander Shkurenko,[a] Jiangtao Jia,[a] Vincent Guillerm,[a] Omar F. Mohammed,[d] Xiaolan Chen,[b] Nanfeng Zheng,[b] Hannu Häkkinen[c] and Mohamed Eddaoudi *[a]

Here we report the synthesis and crystallization of a –COOH-capped *N*-heterocyclic carbene (NHC)-protected Au_{13} cluster. The single-crystal structure of the –COOH-capped NHC-Au_{13} cluster reveals a classic icosahedral core with one Au atom in its center. The icosahedral core is surrounded by five NHC ligands with pseudo C5 symmetry and exposed carboxyls in a pentagonal antiprism fashion. The detailed formula of the Au cluster was identified as Au_{13}(bi-NHC carboxyl)$_5Cl_2$ (hereafter abbreviated as **Au_{13}-c**). The density functional theory (DFT) calculations confirm that **Au_{13}-c** is an electronically stable eight-electron super-atom cluster and elucidate its optical transitions in the UV-Vis range. The **Au_{13}-c** cluster exhibits excellent thermal and chemical stability under bio-relevant conditions. Additionally, this cluster shows a strong red emission in DMF and H_2O with an excellent quantum yield (QY) of 40% and 12.6%, respectively. The high QY of **Au_{13}-c** enables its use in cell imaging on both cancer and noncancerous cells.

Received 10th July 2024
Accepted 27th August 2024

DOI: 10.1039/d4sc04594g

rsc.li/chemical-science

Introduction

In the past few decades, researchers have developed and reported numerous Au nanoclusters (NCs) protected by phosphine, thiol, and alkynyl ligands.[1–5] Multiple studies have explored their potential applications in various fields, including biomedicine and catalysis due to their ultra-small sizes, defined structures, and unique electronic properties.[1–4,6–11] Recently, *N*-heterocyclic carbenes (NHCs) have emerged as valuable ligands due to their strong coordination on the surface of Au NCs as well as nanoparticles (NPs).[12–21] The DFT calculations of the mix-ligand protected $[Au_{11}(PPh_3(NHC)^{i\text{-}Pr})]Cl$ cluster illustrated the weaker connection of the Au phosphine bond compared with the Au carbene bond.[12] Also, the carbene-protected Au_{25} cluster demonstrated better stability compared with the thiol protected Au_{25} cluster.[13] Recently, numerous reports on NHC-protected Au NCs have highlighted their outstanding stabilities, especially for Au_{10}, Au_{11}, Au_{13}, Au_{24}, and Au_{25}.[12–16,18,22–27] Meanwhile, other NCs such as Au_{16}, Au_{23}, and Au_{44} have also been explored in mixed-ligand systems.[28,29] Among them, the Au_{13} cluster co-protected by the bidentate NHC (1,3-bis(1-benzyl-1*H*-benzimidazol-1-ium-3-yl)propane) and bromides showed excellent thermal and biological stability.[23]

The use of NHCs, as stabilizing capping ligands for Au NCs, holds great promise in addressing some challenges such as achieving stable and water-soluble NCs, owing to the possibility of functionalizing these ligands with various groups. It is worth mentioning that very few examples of water-soluble NHC-stabilized metal NPs have been reported, such as sulfonated NHC-stabilized Pt NPs[30] and polyethylene glycol (PEG)-functionalized NHC-protected Au NPs, which showed high stability in a wide range of pH,[31] as well as Au and Pd NPs coordinated by bidentate hybrid NHC–thioether ligands bearing sulfonate or carboxylate moieties.[32] These studies were mainly focused on their application in catalysis. Later, carboxylated NHC-protected Au NPs with good thermal stability were

[a]*Functional Materials Design, Discovery, and Development Research Group (FMD3), Advanced Membranes and Porous Materials Center (AMPM), Division of Physical Sciences and Engineering (PSE), King Abdullah University of Science and Technology (KAUST), Thuwal 23955-6900, Saudi Arabia. E-mail: mohamed.eddaoudi@kaust.edu.sa; Tel: +966 544700025*

[b]*State Key Laboratory for Physical Chemistry of Solid Surfaces, Collaborative Innovation Center of Chemistry for Energy Materials and Department of Chemistry, College of Chemistry and Chemical Engineering, Xiamen University, Xiamen 361005, China*

[c]*Departments of Physics and Chemistry, Nanoscience Center, University of Jyväskylä, FI-40014 Jyväskylä, Finland*

[d]*Advanced Membranes and Porous Materials Center (AMPM), Division of Physical Sciences and Engineering (PSE), King Abdullah University of Science and Technology (KAUST), Thuwal 23955-6900, Saudi Arabia*

† Electronic supplementary information (ESI) available: Synthetic procedures, crystallographic data and analysis, NMR, FTICR-MS, calculations, UV-Vis data and crystallographic structure and data of the **Au_{13}-c** cluster (CIF). CCDC 2249862. For ESI and crystallographic data in CIF or other electronic format see DOI: **https://doi.org/10.1039/d4sc04594g**

reported, which showed potential applications in photoacoustic (PA) imaging.[33] However, these studies have shown that controlling the sizes and achieving the monodispersity of the former Au NPs are difficult. Conversely, the ability to synthesize NCs is more desirable since it allows for more accurate control over their sizes and structures. Synthesizing water-soluble NHC-capped Au NCs still remains a big challenge. Among the water-soluble groups, such as SO_3^- and –OH, the pH tunability and ease of derivatization of carboxylates make them a good choice for functional groups.[33]

Results and discussion

Among several carboxylate-capped NHCs, 1,3-bis(methyl 1-benzylbenzimidazole-5-carboxylate)propane (bi-NHC carboxyl) was selected due to its outstanding thermal stability. In this work, we report the synthesis and characterization of the first –COOH-capped NHC ligand-protected Au_{13} cluster, Au_{13}(bi-NHC carboxyl)$_5Cl_2$ (hereafter abbreviated as **Au_{13}-c**). For the crystallization, in contrast to the recently reported salting-out method used for the crystallization of the –COOH–SH protected Au_{25} cluster,[7] here we have developed a facile way to crystalize our **Au_{13}-c** cluster by adding nitric acid into the DMF solution at 65 °C. Later on, the high thermal and chemical stabilities of the **Au_{13}-c** cluster were investigated. Additionally, its luminescence properties in DMF and H_2O were also explored and deployed in cell imaging.

The detailed synthesis of the **Au_{13}-c** cluster is shown in the ESI,† which also involves the preparation of the bi-NHC carboxyl ligand and bi-NHC carboxyl Au complex. In general, the prepared bi-NHC carboxyl Au complex was dissolved in a NaOH aqueous solvent (2 eq), and after 5 minutes, 10 eq of $NaBH_4$ was introduced (Fig. 1A), and the brown solution rapidly turned red. After aging overnight, 20 μL HCl (12 M) was added, and a red precipitate was collected. Then the collected red precipitate was dissolved in DMF and examined by high-resolution Fourier transform ion cyclotron resonance-mass spectrometry (FTICR-MS). As shown in Fig. 1B, the major peak at ~1785 Da was identified as $H_{10}[Au_{13}$(bi-NHC carboxylate)$_5$-$Cl_2]^{3+}$; the other major peaks at ~2043, 2524, 2695, and 2811 Da were attributed to $H_{12}[Au_{13}$(bi-NHC carboxylate)$_5Cl_2$ + Au(bi-NHC carboxylate)Cl$]^{3+}$, $H_8[Au_{13}$(bi-NHC carboxylate)$_4Cl_3$-$AuH_5]^{2+}$, $H_{10}[Au_{13}$(bi-NHC carboxylate)$_5Cl_2$ + Cl$]^{2+}$, and $H_{10}[Au_{13}$(bi-NHC carboxylate)$_5Cl_2$ + $AuCl_2]^{2+}$, respectively, as shown in Fig. S8.† The electron-counting rule[34] suggests that the **Au_{13}-c** cluster is an eight-electron super atomic system,[35] the same as the previously reported bidentate NHC-protected Au_{13} cluster.[23–25] Fig. 1C shows the UV-Vis spectrum of the **Au_{13}-c** cluster dissolved in aqueous NaOH solution (pH = 14). Four absorption peaks were observed at 304, 330, 425, and 520 nm.

After one week in a 65 °C oven, red single crystals were formed in the HNO_3-DMF solution. The collected red **Au_{13}-c** single crystals (Fig. S1†) were analyzed by single-crystal X-ray diffraction (SCXRD) at 100 K. The **Au_{13}-c** cluster crystallized in the $P2_1/n$ space group, with unit cell parameters $a = 26.064(1)$ Å, $b = 27.538(1)$ Å, $c = 35.319(1)$ Å, $\beta = 91.118(2)°$ (more details in Table S1†). The molecular structure of the **Au_{13}-c** cluster is shown in Fig. 2A. The core of the **Au_{13}-c** cluster is a classic icosahedron with one Au atom in the center. Two chlorides capped the poles of the icosahedron, surrounded by five NHC ligands, giving the cluster pseudo C_5 symmetry with the carboxyls located in a pentagonal antiprism fashion. Compared with former bi-NHC-protected Au_{13} clusters,[23] the average lengths of Au_{Core}–Au_{Shell}, Au_{Core}–Au_C, and Au_{Core}–Au_{Hal} bonds are comparatively shorter, as shown in Table S2.† Multiple C–

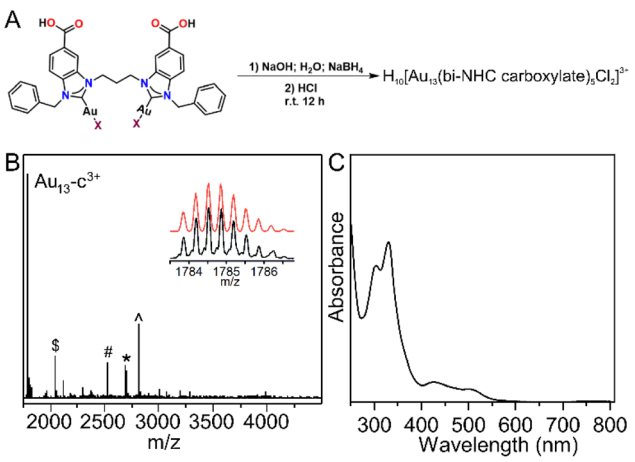

Fig. 1 (A) Preparation of the **Au_{13}-c** cluster; (B) FTICR-MS profile of the crude reaction mixture dissolved in DMF. From right to left: ($) H_{12}[**Au_{13}-c** + Au(NHC)Cl$]^{3+}$, (#) $H_8[Au_{13}(NHC)_4Cl_3Au_1H_5]^{2+}$, (*) H_{10}[**Au_{13}-c** + Cl$]^{2+}$, (^) H_{10}[**Au_{13}-c** + $AuCl_2]^{2+}$. Inset: simulated (red curve) and experimental (black curve) isotope distribution patterns; (C) UV-Vis spectrum recorded of the **Au_{13}-c** cluster.

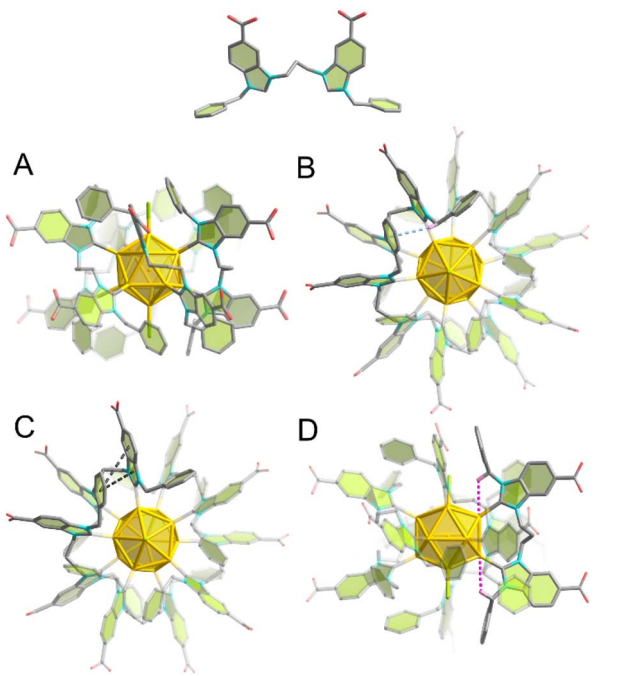

Fig. 2 (A) Side view of the **Au_{13}-c** cluster; multiple weak interactions of the **Au_{13}-c** cluster. (B) C–H···π interaction; (C) π–π interaction; (D) C–H···Au interaction. Color codes: gold, Au; blue, Cl; aqua, N; light red, O; grey, C and rose, H. Other hydrogen atoms were omitted for clarity.

H···Au, C–H···π and π–π interactions (Tables S3–S5†) between the bi-NHC ligands additionally stabilize the **Au_{13}-c** cluster.

A total of 10 carboxyl groups are present around the surface of the **Au_{13}-c** cluster, 3 of which are fully deprotonated and balancing the charge of the metal core. The fourth carboxylic group is partially deprotonated (2/3) and its charge is balanced by the presence of Na^+ cations. This partial deprotonation causes positional disorder of the bi-NHC ligand over two positions depending on the presence or absence of sodium cations. Each sodium cation coordinates three carboxylate groups of three adjacent **Au_{13}-c** clusters and three water molecules. The **Au_{13}-c** clusters are self-assembled into two-dimensional layers parallel to the crystallographic plane[36] mainly *via* strong O–H···O hydrogen bonding (Table S6†) between the carboxyl groups themselves or carboxyl groups and water, but also due to coordination by sodium (Fig. S9A†). The layers are packed along <010> due to van der Waals interactions.

We believe that the presence of multiple weak intramolecular interactions within the **Au_{13}-c** cluster, such as π···π, C–H···Au, and C–H···π interactions between NHC ligands or between NHC ligands and gold atoms, contributes to its photoluminescence properties (Fig. 2B–D). The luminescence decay times of the **Au_{13}-c** cluster dissolved in water (pH = 14) or DMF (Fig. S10†) were found to be 792 and 1416 ns, respectively. The shorter lifetime in water is caused by the stronger non-radiative transitions.

We studied the electronic structure and optical properties of the **Au_{13}-c** cluster using the density functional theory (DFT) method, as implemented in the GPAW software[37] (see the ESI† for further details). The projected electronic density of states (PDOS) in the ground state shows a prominent energy gap (1.97 eV) between the highest occupied (HOMO) and lowest unoccupied (LUMO) molecular orbital states (Fig. 3B), reflecting the high electronic stability of the cluster. As expected from the chemical composition, the symmetries of the frontier orbitals show a clear eight-electron super-atomic character, where the three uppermost occupied states have a dominant P symmetry and the lowest unoccupied states have D symmetry (see the real-space visualization of several frontier orbitals in Fig. S11†). Notably, the three P states are split, due to the Cl atoms in one of the five-fold symmetry axes of the gold core (Fig. 2B).

We calculated the optical absorption spectrum using the linear-response time-dependent DFT, and the results are shown in Fig. 3A. The spectrum shows four clear peaks (labelled 1–4 in Fig. 3A), similar to the experimental data in Fig. 1C; as shown in Table 1, the peak positions are in semi-quantitative agreement. The peaks were analyzed using the dipole transition contribution maps (DTCMs) shown in Fig. 3.

Peak 1 is composed of super atomic metal–metal transitions from P-symmetric HOMO/HOMO−1 states to D-symmetric LUMO/LUMO+1 states, although it should be noted that the LUMO and LUMO+1 states have some weight in the ligand layer as well (Fig. 3). Peak 2 has two clear contributions: one from a group of states having weight at the metal–ligand interface (HOMO−3 to HOMO−5, appearing as F-symmetric states in the

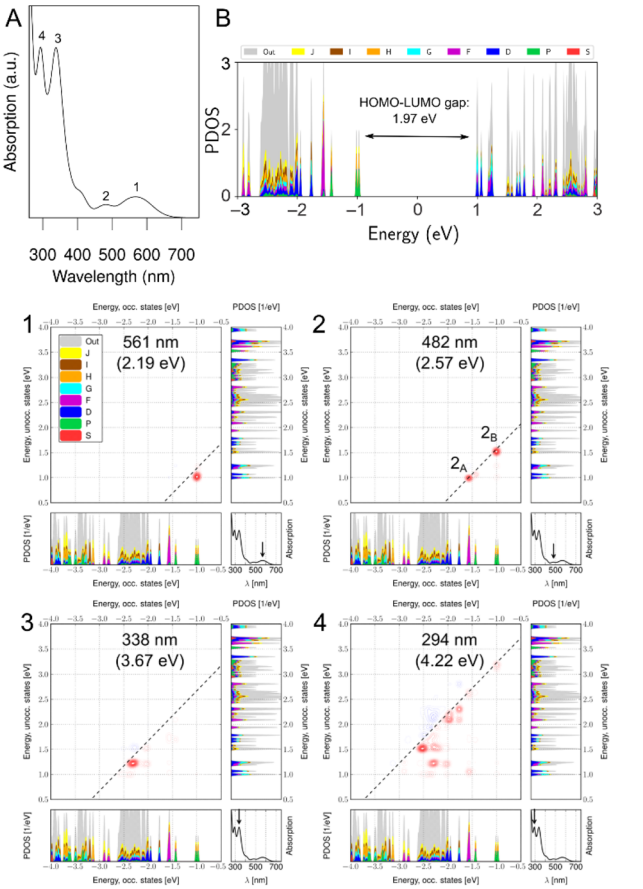

Fig. 3 (A) Calculated optical absorption spectrum and (B) projected electronic density of states (PDOS) of the **Au_{13}-c** cluster. The four absorption peaks labeled 1–4 in (A) were also found in the experimental spectrum (Fig. 2D). The different colors in (B) denote different angular momenta used in the projection with respect to the cluster's center of mass. The label "out" denotes electron densities that could not be described with angular momenta up to J symmetry. The HOMO–LUMO gap was centered at 0 eV. Dipole transition contribution maps of the $H_{10}[Au_{13}(bi\text{-}NHC\ carboxyl)_5Cl_2]^{3+}$ cluster were analyzed for the four peaks labeled in (A). The upper left panel shows the strengthening (red contours) and screening (blue contours) contributions as being decomposed into transitions between Kohn–Sham states that are represented as the projected density of states similar to (B). Occupied states are shown in the lower left panel and unoccupied states in the upper right panel. The lower right panel shows the absorption spectrum and labels the analyzed peak with an arrow. In (B) the two main contributions have been labeled as 2_A and 2_B.

Table 1 Calculated and measured peaks 1–4 in the optical spectrum of the **Au_{13}-c** cluster

	Calculated		Experimental	
	nm	eV	nm	eV
1	561	2.19	520	2.38
2	482	2.57	425	2.92
3	338	3.67	330	3.76
4	294	4.22	304	4.08

projection) to LUMO/LUMO+1 states, and another from the P-symmetric HOMO/HOMO−1 states to the predominantly ligand states LUMO+7 to LUMO+10 (Fig. S12†). This peak corresponds to the 420 nm excitation used to study the fluorescence, as discussed above. Peak 3 has contributions from Au(d) and ligand states, and peak 4 has the most collective character, involving close to 10 contributions in a broad energy range in both occupied and unoccupied manifolds. A more detailed analysis of the origin of the peaks 3 and 4 using atom projected density of states (shown in Fig. S13†) shows that the ligand contributions to peak 3 come from the side and the head groups, but not from carboxylic or linker groups of the ligand. The same analysis confirms that peak 4 has more spread contributions from all structure parts. Metal atoms contribute to both peaks 3 and 4.

We chose two absorptions at 425 and 520 nm to identify the structure during stability tests. First, we checked the stability of the **Au_{13}-c** cluster in a wide pH range; because of the carboxyl groups, the structure showed excellent stability in the pH range from 7 to 14 even after 12 h, while, at pH = 1 and 4, the **Au_{13}-c** cluster would aggregate due to the strong hydrogen bonding between clusters. Moreover, the UV-Vis spectrum of the **Au_{13}-c** cluster showed no discernible change after 12 h treatment with H_2O_2, $NaBH_4$, and biological media such as saline and glutathione (GSH), and under 65 °C, as shown in Fig. S14.† It was observed that with introducing carboxylate, the thermal stability decreased from 100 to 65 °C.[23,33] For the GSH, the side –SH group didn't influence the stability of the **Au_{13}-c** cluster, and to further explore the stability of the **Au_{13}-c** cluster against thiols, 1-dodecanethiol was selected to investigate the possibility for the end –SH group to replace the chloride anions (Cl^-). A replacement experiment was performed, as shown in Fig. S15B and C,† and according to the calculated UV-Vis spectra, there's no shift in the UV-Vis range before and after the replacement experiment. Also, no new signal was observed in the IR spectra (Fig. S15D and E†). Therefore, these results confirm that no Au–S bond formation was observed during the replacement process, which indicates that this **Au_{13}-c** cluster possesses a robust surface against thiols.

The photoluminescence properties of the **Au_{13}-c** cluster were also analyzed. Based on Fig. 4C, we chose 420 nm as the excitation wavelength and measured the emission of the solid **Au_{13}-c** cluster, which showed a red emission at 700 nm. Similarly, upon dissolving in DMF, the **Au_{13}-c** cluster exhibited a blue shift at 694 nm; conversely upon dispersing in water, it exhibited a red shift with an emission at 710 nm. Upon excitation at 420 nm, the **Au_{13}-c** cluster exhibited a clear red emission in DMF with an excellent quantum yield (QY) of 40.0%; the modified crystals showed a QY of 34.9%. The QY of the **Au_{13}-c** cluster in water was 12.6%, which is at least 6-fold higher than those of DHLA-Au NCs (0.6%),[38] DPA-capped Au NCs (1.3%),[39] RNase-A@Au NCs (1.9%)[40] and PDMAEMA-AuNCs (3.5%)[41] (Table S7†). We believe that the higher QY in DMF was attributed to the interactions between –COOH groups and DMF molecules. Furthermore, the QY of the Au_{13} cluster was measured, showing 16% when dissolved in DMF and 0.8% for the crystals respectively, which are much lower compared with

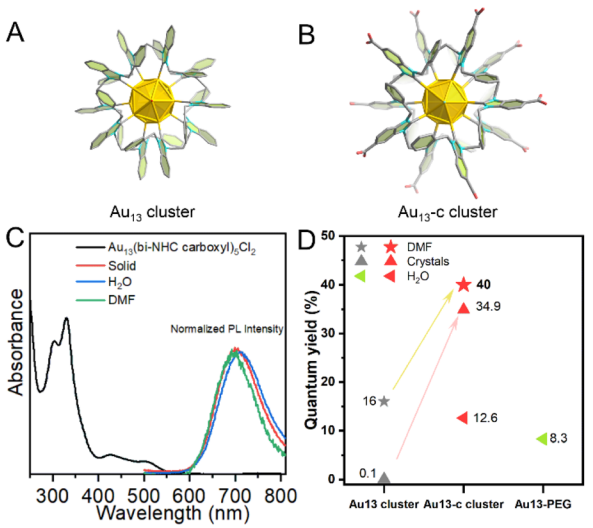

Fig. 4 The structures of Au_{13} (A) and **Au_{13}-c** clusters (B); (C) the UV-Vis and normalized PL intensity emission spectra of the **Au_{13}-c** cluster with excitation at 420 nm; (D) the QY comparison of Au_{13}, **Au_{13}-c** and Au_{13}-PEG under different conditions.

those of the **Au_{13}-c** cluster, as shown in Fig. 4D and Fig. S17.† (ref. 23) The strong photoluminescence (PL) enhancement of the **Au_{13}-c** cluster was considered as a contribution of the –COOH groups. We measured the QY of the **Au_{13}-c** cluster dissolved in an aqueous NaOH solution (pH = 14), and a value of 2.7% was detected; additionally, the QYs of two types of crystals were measured. Compared with the modified crystals connected through 6 hydrogen bonds, the QY of the former crystal with Na^+ was only 8.2%. These results both suggest the significant enhancement by the –COOH groups.

To take advantage of the **Au_{13}-c** properties such as ultrasmall molecular size, excellent stability, and outstanding photoluminescence, we intended to further explore its application in cell imaging (Table S7†).

First, in order to impart biocompatibility and stealth properties to the **Au_{13}-c** cluster surface for biomedical applications,[31] SH–PEG–NH_2 was applied to form –NH–CO– bonds with surface carboxyl groups to form the Au_{13}-PEG cluster. IR measurements confirmed the coordination of SH–PEG–NH_2 *via* the appearance of clear signals at 3455 and 2880 cm^{-1} (Fig. S16†). The Au_{13}-PEG shows absorptions at 303 and 338 nm, with excitation at 338 nm, and it shows an emission at 750 nm, with a QY of 8.3% in H_2O. The biocompatibility of the Au_{13}-PEG was evaluated by testing the viability of live cells using the 3-(4,5-dimethylthiazol-2)-2,5-diphenyltetrazolium bromide (MTT) assay. Cells from 4T1 (mouse breast cancer cell) and L929 (normal mouse breast cell) were used to evaluate the ability of the Au_{13}-PEG to light up affected parts of cancerous and noncancerous cells. No reduction in viability was observed after incubation with the Au_{13}-PEG, even at a concentration of 500 μg mL^{-1} of 4T1 cells, and at least 84% of L929 cells remained viable at 36 μg mL^{-1}, suggesting good biocompatibility (Fig. S18†). Moreover, the microscopic observation detected no morphological changes that would indicate adverse effects of **Au_{13}-c** cluster exposure. Fig. 5 and S19† show confocal images of normal mouse

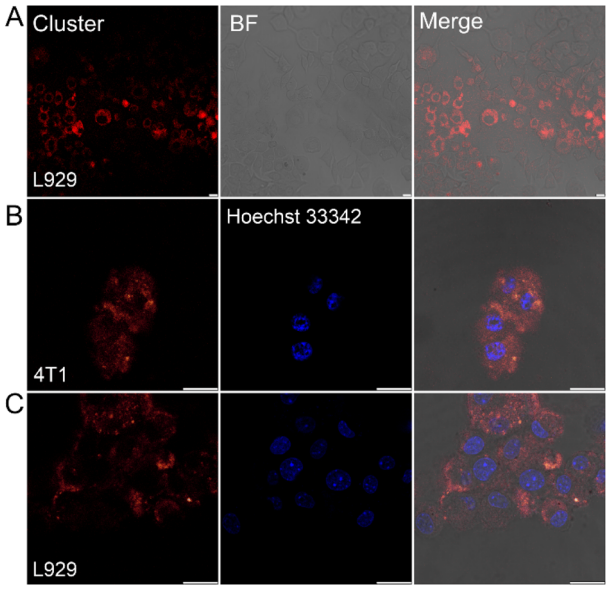

Fig. 5 Confocal luminescence microscopy images of pretreated 4T1 and L929 cells. (A) Incubated for 48 h, (B) 4T1 cells, (C) L929 cells cultured in the presence of Hoechst 33342 (10 μM) and the Au13-PEG cluster (75 μg mL^{-1}) for 48 h. The Hoechst 33342 dye was used to stain the cell nucleus (scale bar = 20 μm).

fibroblast cells (L929) separately stained with the Au_{13}-PEG for 24 and 48 h.

In contrast to previously reported water-soluble Au NCs, such as BSA-Au NCs, which localize in a much larger volume encompassing both the cell membrane and cytoplasm of human breast cancer cells (MCF7) but were primarily localized on the cell membrane of normal human breast cells (MCF10A).[42] A similar situation was also observed for doxorubicin-loaded Au NCs.[42,43] Additionally, it should be noted that the non-carboxyl group-capped Au_{13} cluster was mainly localized onto the cell membrane of HeLa cells.[23] Surprisingly, even in noncancerous cells (L929), a significant amount of Au_{13}-PEG was found in both the membrane and cytoplasm, with a small fraction even detected within the nucleus. Furthermore, Hoechst 33342 was used as a nuclear dye; as shown in Fig. 5 and S20–S22,† the photoluminescence of the dye did not interfere with the emission of the present Au_{13}-PEG.

Conclusions

In conclusion, we have successfully developed an approach to synthesize and a facile way to crystallize the first –COOH-capped NHC-protected **Au_{13}-c** cluster, which was identified as an eight-electron super-atomic system. This **Au_{13}-c** cluster showed excellent thermal, thiol, and bio-relevant agent stabilities, coupled with an excellent quantum yield (40% in DMF and 12.6% in water). We explored the performance of the functionalized **Au_{13}-c** cluster in cell imaging and successfully demonstrated its excellent intracellular photoluminescence in 4T1 cells and even noncancerous cells (L929). These results unambiguously demonstrate the great potential of the –COOH agent-capped NHC-protected, ultra-stable Au clusters. In addition to the biochemical applications, the introduced –COOH groups on NHC ligands can also pave the way for their use as building units in the synthesis of metal–organic frameworks (MOFs) *via* their coordination with other metals for further topology research; further studies are underway in our laboratory.

Data availability

Data supporting this study are included within the article and/or supporting materials.†

Author contributions

M. E. and N. F. Z. conceived the project. X. T. Y. carried out the synthesis and characterization of the Au_{13} and **Au_{13}-c** clusters. Z. C. Y. and X. Y. H. did the cell-imaging analysis. S. M. performed the DFT calculations. J. X. W. and H. W. performed the quantum yield calculation of Au_{13} and **Au_{13}-c** clusters, and Au_{13}-PEG. A. S. analysed the X-ray crystal of the **Au_{13}-c** cluster. All the authors wrote the paper, supplementary methods, and related materials.

Conflicts of interest

The authors declare no competing financial interest.

Acknowledgements

Research reported in this publication was supported by the King Abdullah University of Science and Technology (KAUST). The computational work at the University of Jyväskylä (JYU) was supported by the Academy of Finland (grant 351582) and by the excellence funding from the JYU Rector.

References

1 Z. Lei, X. K. Wan, S. F. Yuan, Z. J. Guan and Q. M. Wang, *Acc. Chem. Res.*, 2018, **51**, 2465–2474.
2 P. D. Jadzinsky, G. Calero, C. J. Ackerson, D. A. Bushnell and R. D. Kornberg, *Science*, 2007, **318**, 430–433.
3 Y. Shichibu and K. Konishi, *Small*, 2010, **6**, 1216–1220.
4 Y. T. Cao, T. Y. Liu, T. K. Chen, B. H. Zhang, D. E. Jiang and J. P. Xie, *Nat. Commun.*, 2021, **12**, 3212.
5 R. C. Jin, C. J. Zeng, M. Zhou and Y. X. Chen, *Chem. Rev.*, 2016, **116**, 10346–10413.
6 Y. X. Du, H. T. Sheng, D. Astruc and M. Z. Zhu, *Chem. Rev.*, 2019, **120**, 526–622.
7 W. D. Tian, W. D. Si, S. Havenridge, C. K. Zhang, Z. Wang, C. M. Aikens, C. H. Tung and D. Sun, *Sci. Bull.*, 2023, **69**, 40–48.
8 G. Yang, Z. P. Wang, F. L. Du, F. Y. Jiang, X. Yuan and J. Y. Ying, *J. Am. Chem. Soc.*, 2023, **145**, 11879–11898.
9 J. Yang, F. Yang, C. S. Zhang, X. B. He and R. c. Jin, *ACS Mater. Lett.*, 2022, 1279–1296.
10 M. F. Matus and H. Häkkinen, *Nat. Rev. Mater.*, 2023, **8**, 372–389.

11 M. Z. Zhu, E. Lanni, N. Garg, M. E. Bier and R. C. Jin, *J. Am. Chem. Soc.*, 2008, **130**, 1138–1139.
12 M. R. Narouz, K. M. Osten, P. J. Unsworth, R. W. Y. Man, K. Salorinne, S. Takano, R. Tomihara, S. Kaappa, S. Malola, C. T. Dinh, J. D. Padmos, K. Ayoo, P. J. Garrett, M. Nambo, J. H. Horton, E. H. Sargent, H. Hakkinen, T. Tsukuda and C. M. Crudden, *Nat. Chem.*, 2019, **11**, 419–425.
13 H. Shen, G. C. Deng, S. Kaappa, T. D. Tan, Y. Z. Han, S. Malola, S. C. Lin, B. K. Teo, H. Hakkinen and N. F. Zheng, *Angew. Chem., Int. Ed.*, 2019, **58**, 17731–17735.
14 M. R. Narouz, S. Takano, P. A. Lummis, T. I. Levchenko, A. Nazemi, S. Kaappa, S. Malola, G. Yousefalizadeh, L. A. Calhoun, K. G. Stamplecoskie, H. Hakkinen, T. Tsukuda and C. M. Crudden, *J. Am. Chem. Soc.*, 2019, **141**, 14997–15002.
15 P. Luo, X. J. Zhai, S. Bai, Y. B. Si, X. Y. Dong, Y. F. Han and S. Q. Zang, *Angew. Chem., Int. Ed.*, 2023, e202219017.
16 J. Sun, X. Tang, J. Tang, Y. Zhang, Z. Li, Chaolumen, S. Guo and H. Shen, *Inorg. Chem.*, 2023, **62**, 5088–5094.
17 J. Liu, Y. Sato, V. K. Kulkarni, A. I. Sullivan, W. Zhang, C. M. Crudden and J. E. Hein, *Chem. Sci.*, 2023, **14**, 10500–10507.
18 A. I. Sullivan, J. F. DeJesus, S. Malola, S. Takano, T. Tsukuda, H. Häkkinen and C. M. Crudden, *Chem. Mater.*, 2023, **35**, 2790–2796.
19 C. A. Smith, M. R. Narouz, P. A. Lummis, I. Singh, A. Nazemi, C. H. Li and C. M. Crudden, *Chem. Rev.*, 2019, **119**, 4986–5056.
20 M. Bevilacqua, M. Roverso, S. Bogialli, C. Graiff and A. Biffis, *Inorg. Chem.*, 2023, **62**, 1383–1393.
21 E. L. Albright, T. I. Levchenko, V. K. Kulkarni, A. I. Sullivan, J. F. DeJesus, S. Malola, S. Takano, M. Nambo, K. Stamplecoskie, H. Hakkinen, T. Tsukuda and C. M. Crudden, *J. Am. Chem. Soc.*, 2024, **146**, 5759–5780.
22 P. A. Lummis, K. M. Osten, T. I. Levchenko, M. Sabooni Asre Hazer, S. Malola, B. Owens-Baird, A. J. Veinot, E. L. Albright, G. Schatte, S. Takano, K. Kovnir, K. G. Stamplecoskie, T. Tsukuda, H. Hakkinen, M. Nambo and C. M. Crudden, *JACS Au*, 2022, **2**, 875–885.
23 H. Shen, S. J. Xiang, Z. Xu, C. Liu, X. H. Li, C. F. Sun, S. C. Lin, B. K. Teo and N. F. Zheng, *Nano Res.*, 2020, **13**, 1908–1911.
24 P. Luo, S. Bai, X. Wang, J. Zhao, Z. N. Yan, Y. F. Han, S. Q. Zang and T. C. W. Mak, *Adv. Opt. Mater.*, 2021, **9**, 2001936–2001941.
25 H. Yi, K. M. Osten, T. I. Levchenko, A. J. Veinot, Y. Aramaki, T. Ooi, M. Nambo and C. M. Crudden, *Chem. Sci.*, 2021, **12**, 10436–10440.
26 V. K. Kulkarni, B. N. Khiarak, S. Takano, S. Malola, E. L. Albright, T. I. Levchenko, M. D. Aloisio, C.-T. Dinh, T. Tsukuda, H. Häkkinen and C. M. Crudden, *J. Am. Chem. Soc.*, 2022, **144**, 9000–9006.
27 E. L. Albright, S. Malola, S. I. Jacob, H. Yi, S. Takano, K. Mimura, T. Tsukuda, H. Häkkinen, M. Nambo and C. M. Crudden, *Chem. Mater.*, 2024, **36**, 1279–1289.
28 H. Shen, Q. Y. Wu, S. Malola, Y. Z. Han, Z. Xu, R. X. Qin, X. K. Tang, Y. B. Chen, B. K. Teo, H. Hakkinen and N. F. Zheng, *J. Am. Chem. Soc.*, 2022, **144**, 10844–10853.
29 H. Shen, Z. Xu, M. S. A. Hazer, Q. Y. Wu, J. Peng, R. X. Qin, S. Malola, B. K. Teo, H. Hakkinen and N. F. Zheng, *Angew. Chem., Int. Ed.*, 2020, **60**, 3752–3758.
30 E. A. Baquero, S. Tricard, J. C. Flores, E. de Jesús and B. Chaudret, *Angew. Chem., Int. Ed.*, 2014, **53**, 13220–13224.
31 M. J. MacLeod and J. A. Johnson, *J. Am. Chem. Soc.*, 2015, **137**, 7974–7977.
32 A. Ferry, K. Schaepe, P. Tegeder, C. Richter, K. M. Chepiga, B. J. Ravoo and F. Glorius, *ACS Catal.*, 2015, **5**, 5414–5420.
33 K. Salorinne, R. W. Y. Man, C. H. Li, M. Taki, M. Nambo and C. M. Crudden, *Angew Chem. Int. Ed. Engl.*, 2017, **56**, 6198–6202.
34 M. Walter, J. Akola, O. Lopez-Acevedo, D. P. Jadzinsky, G. Calero, J. C. Ackerson, L. R. Whetten, H. Gronbeck and H. Hakkinen, *Proc. Natl. Acad. Sci. U. S. A.*, 2008, **105**, 9157–9162.
35 J. Z. Yan, B. K. Teo and N. F. Zheng, *Acc. Chem. Res.*, 2018, **51**, 3084–3093.
36 P. H. Lin, S. C. Sheu, C. W. Chen, S. C. Huang and B. R. Li, *Talanta*, 2022, **241**, 123187.
37 J. Enkovaara, C. Rostgaard, J. J. Mortensen, J. Chen, M. Dułak, L. Ferrighi, J. Gavnholt, C. Glinsvad, V. Haikola, H. A. Hansen, H. H. Kristoffersen, M. Kuisma, A. H. Larsen, L. Lehtovaara, M. Ljungberg, O. Lopez-Acevedo, P. G. Moses, J. Ojanen, T. Olsen, V. Petzold, N. A. Romero, J. Stausholm-Møller, M. Strange, G. A. Tritsaris, M. Vanin, M. Walter, B. Hammer, H. Häkkinen, G. K. H. Madsen, R. M. Nieminen, J. K. Nørskov, M. Puska, T. T. Rantala, J. Schiøtz, K. S. Thygesen and K. W. Jacobsen, *J. Phys.: Condens.Matter*, 2010, **22**, 253202.
38 L. Shang, N. Azadfar, F. Stockmar, W. Send, V. Trouillet, M. Bruns, D. Gerthsen and G. U. Nienhaus, *Small*, 2011, **7**, 2614–2620.
39 L. Shang, R. M. Dorlich, S. Brandholt, R. Schneider, V. Trouillet, M. Bruns, D. Gerthsen and G. U. Nienhaus, *Nanoscale*, 2011, **3**, 2009–2014.
40 W. Wang, Y. Kong, J. Jiang, Q. Xie, Y. Huang, G. Li, D. Wu, H. Zheng, M. Gao, S. Xu, Y. Pan, W. Li, R. Ma, M. X. Wu, X. Li, H. Zuilhof, X. Cai and R. Li, *Angew. Chem., Int. Ed.*, 2020, **59**, 22431–22435.
41 S. C. Zhou, L. Gustavsson, G. Beaune, S. Chandra, J. Niskanen, J. Ruokolainen, J. V. I. Timonen, O. Ikkala, B. Peng and R. Ras, *Angew. Chem., Int. Ed.*, 2023, e202312679.
42 S. Chattoraj and K. Bhattacharyya, *J. Phys. Chem. C*, 2014, **118**, 22339–22346.
43 S. Chattoraj, A. Amin, B. Jana, S. Mohapatra, S. Ghosh and K. Bhattacharyya, *ChemPhysChem*, 2016, **17**, 253–259.